



This is the accepted manuscript made available via CHORUS, the article has been published as:

Relationship between frequency and deflection angle in the DNA prism

Zhen Chen and Kevin D. Dorfman

Phys. Rev. E **87**, 012723 — Published 28 January 2013

DOI: [10.1103/PhysRevE.87.012723](https://doi.org/10.1103/PhysRevE.87.012723)

Relationship Between Frequency and Deflection Angle in the DNA Prism

Zhen Chen and Kevin D. Dorfman*

*Department of Chemical Engineering and Materials Science,
University of Minnesota - Twin Cities,
421 Washington Ave SE, Minneapolis, MN 55455, USA*

Abstract

The DNA prism is a modification of the standard pulsed-field electrophoresis protocol to provide a continuous separation, where the DNA are deflected at an angle that depends on their molecular weight. The standard switchback model for the DNA prism predicts a monotonic increase in the deflection angle as a function of the frequency for switching the field until a plateau regime is reached. However, experiments indicate that the deflection angle achieves a maximum value before decaying to a size-independent value at high frequencies. Using Brownian dynamics simulations, we show that the maximum in the deflection angle is related to the reorientation time for the DNA and the decay in deflection angle at high frequencies is due to inadequate stretching. The generic features of the dependence of the deflection angle on molecular weight, switching frequency, and electric field strength explain a number of experimental phenomena.

PACS numbers: 82.45.Tv, 87.15.Tt

* dorfman@umn.edu

I. INTRODUCTION

One of the goals of microfluidics research is displacing agarose gel electrophoresis as the standard method for separating DNA, in particular for long DNA in excess of tens of kilobase pairs (kbp). Despite intense research over the past decade [1–7], developing a replacement technology has proven more challenging than first anticipated. Supplanting agarose gel electrophoresis as a preparative method requires shifting the microfluidic separation from a batch mode to a continuous mode, such that the amount of DNA processed per unit time starts to approach the quantity typically loaded into a gel. A number of such strategies exist, including asymmetric Brownian ratchets [8–11], deterministic lateral displacement [12] and the anisotropic nanofilter array [13]. Perhaps the most promising of all of the methods for separating long DNA is the so-called “DNA prism” [14], which has already found utility as a component of an integrated lab-on-a-chip for pathogen detection [15]. As we see in Fig. 1, the DNA prism protocol produces a deflection angle θ that is a function of the molecular weight of the DNA. Thus, the DNA can be continuously fed to the inlet and collected at different locations in the outlet. The moniker “DNA prism” refers to the way in which a stream of DNA is split into different “rays” through the device, in a manner that inspires analogies with the diffraction of light [14]. However, the physics of DNA separations in the DNA prism are considerably more complicated than the optics of a conventional prism, and a number of puzzling experimental results exist [14, 16]. In this paper, we use Brownian dynamics simulations to develop a basic understanding of transport in the DNA prism, thereby allowing us to explain these experimental results.

The basis of the DNA prism is a clever modification of the clamped homogeneous electric field (CHEF) method for pulsed field gel electrophoresis [18]. In CHEF electrophoresis, an electric field of constant strength E periodically alternates between an angle of zero and an obtuse angle ϕ . The field oscillations are normally a square wave with frequency f , where the field at zero angle is applied for $(2f)^{-1}$ seconds followed by application of the field at obtuse angle ϕ for the same amount of time. In CHEF electrophoresis, the DNA move at an angle $\phi/2$, but their migration speed depends on molecular weight. The origin of the separation is the time required for the DNA to reorient in the direction of the applied electric field after the direction of the electric field changes [19]. The smaller DNA reorient more quickly, and thus have higher mobilities. The idea behind the DNA prism is to convert the

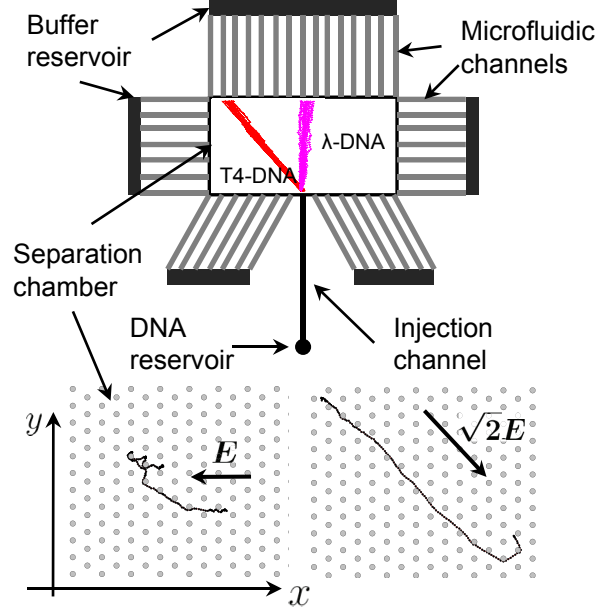


FIG. 1. (color online) Continuous separation as a function of molecular weight in the DNA prism. The separation takes place in the separation chamber, which contains the array of posts seen in the simulation snapshots in the lower portion of the figure. The trajectories seen in the figure correspond to 12 simulations of T4 DNA (red, deflected towards the upper left) and λ DNA (purple, minimally deflected) at a dimensionless frequency $f = 0.01428$ and a Péclet number $Pe = 2$. The details of these simulations and the definition of the parameters are discussed in §III. The surrounding microfluidic channels illustrate the microfluidic approach to implement tunable, uniform electric fields [17]. The simulation snapshots show the reorientation of a T4 DNA molecule when the electric field changes from $\mathbf{E}_2 = E_0(\mathbf{i}_x - \mathbf{i}_y)$ to $\mathbf{E}_1 = -E_0\mathbf{i}_x$ (bottom left) and vice versa (bottom right). Note that the negatively charged DNA migrates to the opposite direction of \mathbf{E} .

CHEF separation from a batch mode to a continuous mode by breaking the symmetry of the applied field. In the DNA prism, an electric field of strength E_1 is applied for some time t_1 , followed by a second field E_2 applied for some time t_2 at an angle ϕ relative to E_1 . Similar to CHEF electrophoresis, experiments in the DNA prism [14, 16] use a square wave for the pulsed field with two different electric field strengths. If the separation is successful, the DNA move at deflection angles $\theta = \theta(N)$ that depend on the DNA molecular weight, N . The DNA also move at different speeds, but these speeds are only relevant during the startup of the separation.

In principle, one could apply the DNA prism protocol in an agarose gel using the standard CHEF apparatus. However, the DNA prism has only been used in microfluidic devices to take advantage of the faster reorientation times and the ability to inject a thin stream of DNA at the inlet. The pioneering DNA prism device [14] used DNA in the hundreds of kilobase pair range and an array of posts for the separation matrix; recall that a post array already exhibits substantial advantages over agarose gel electrophoresis in the standard CHEF mode [20]. Recently, the DNA prism has been implemented using a colloidal crystal [16, 21, 22] as the separation matrix and relatively short DNA in the kilobase to tens of kilobase pair range. All of these microfluidic separations take advantage of a device design [17], sketched in Fig. 1, that produces tunable, uniform electric fields across the array. The microchannels at the perimeter of the separation chamber serve a dual purpose, providing both the uniform electric field and collection points for the fractionated DNA. As we indicate in Fig. 1, we will focus here on understanding the DNA prism in a post array [14], using an angle $\phi = 135^\circ$ and a $\sqrt{2}$ ratio of electric field strengths [16].

Although the DNA prism is now established as a separation method [14–16, 21, 22], the operation of the device is more complicated than one would expect from an extrapolation of the theory for pulsed field gel electrophoresis in a post array [23] to the DNA prism protocol. For example, the simple switchback model of the DNA prism [6, 21] reviewed in §II predicts a monotonic increase in the deflection angle θ as a function of the frequency of the changing electric field, with an eventual plateau in the direction of the stronger electric field at high frequencies. However, experiments [16] indicate a maximum in the deflection angle, with an eventual decrease to a molecular-weight independent deflection angle at high frequencies. There also exists unexplained “band shifting” behavior as the switching frequency changes [14].

In this contribution, we use Brownian dynamics simulations to explain these otherwise puzzling experimental results [14, 16]. Brownian dynamics simulations of DNA electrophoresis in post arrays [24–32] have proven to be a powerful tool for understanding the basic physics of the separation process. If one correctly accounts for the insulating nature of most microfluidic media, Brownian dynamics simulations can yield semi-quantitative agreement with experimental data for the microscale transport of long DNA in post arrays [31] even though the model does not include any explicit electrohydrodynamic effects [33, 34]. As we will see, Brownian dynamics simulations are accurate enough to develop a basic understand-

ing of transport in the DNA prism, which we encapsulate in a “ θ - f ” plot that connects the deflection angle θ of the DNA to the frequency f of the square wave for the electric field [16]. Elucidating the generic features of the θ - f plot allows us to rationalize existing experimental results and provide guidelines for further device development. By examining how the deflection angle is affected by the electric field strength, pulse frequency and molecular weight, we will see that it is relatively easy to determine a combination of parameters that yield the high resolution separation seen in Fig. 1.

II. SWITCHBACK MODEL FOR THE DNA PRISM

Before moving onto the simulations, let us first recall the predictions of the switchback model of pulsed field gel electrophoresis [36] when applied to the DNA prism [6, 21]. We should keep in mind that the switchback model [36] is only a crude approximation for pulsed field DNA electrophoresis, since it does not account for the redistribution of the tension inside the chain when the electric field changes direction [37, 38]. Rather, we simply assume that the DNA is immobilized for some time t^{or} while it reorients in the direction of the new electric field. For the remainder of the square wave in a given direction, $(2f)^{-1} - t^{\text{or}}$, the DNA moves through the matrix with a velocity $v_{i,j} = \mu_{i,j}E_j$, where $\mu_{i,j}$ is the electrophoretic mobility of the DNA of size i when it moves through the matrix under an electric field vector \mathbf{E}_j , where $E_j = |\mathbf{E}_j|$ and $j = (1,2)$ is the part of the square wave. We arbitrarily choose $E_2 > E_1$. In this simple model, the displacement of the DNA of size i during a pulse j is

$$\mathbf{d}_j = \begin{cases} -\mu_{i,j}\mathbf{E}_j \left(\frac{1}{2f} - t_j^{\text{or}} \right) & \text{if } 2ft_j^{\text{or}} < 1 \\ 0 & \text{otherwise} \end{cases} \quad (1)$$

The deflection angle θ for this DNA size is then defined as

$$\cos \theta \equiv \frac{(\mathbf{d}_1 + \mathbf{d}_2) \cdot \mathbf{i}_x}{|\mathbf{d}_1 + \mathbf{d}_2|} \quad (2)$$

where \mathbf{i}_x is a unit vector in the x -direction.

To make further progress, we need to consider the reorientation time. Reorientation is a complicated process [19]. Indeed, it is not always easy to determine whether the reorientation process is led by the head/tail of the DNA or internal hernia formation [39, 40]. Keeping in mind the simplicity of the model thus far, we will only consider equivalently simple

reorientation models. In the simplest approach, we can assume that the DNA simply turns the corner via free solution electrophoresis with an effective electric field E_j ,

$$t_j^{\text{or}} = \frac{L_i}{\mu_0 E_j} \quad (3)$$

where L_i is the contour length of the DNA and μ_0 is the free solution electrophoretic mobility. A more detailed model [23]

$$t_j^{\text{or}} = c \frac{L_i}{\mu_0 E_j} \quad (4)$$

includes a multiplicative factor

$$c \equiv \frac{\ln(1/|\cos \phi|)}{1 - |\cos \phi|} \quad (5)$$

that accounts for the reduction in the DNA velocity due to the angle between the old electric field direction and the new electric field direction [41].

This switchback model makes relatively simple predictions for the deflection angle as a function of the frequency. As the frequency increases from some very low value, the reorientation time in Eq. (1) makes an increasingly important contribution to the deflection angle. Overall, we would expect to see a monotonic increase in the deflection angle with frequency [6, 21] until we reach the point where $t_2^{\text{or}} < (2f)^{-1} < t_1^{\text{or}}$. In this regime, the DNA has time to orient in the strong electric field \mathbf{E}_2 . However, there is insufficient time to reorient when the field switches back to the weaker electric field \mathbf{E}_1 . As a result, the switchback model predicts that all of the DNA will move along the direction of the stronger electric field, albeit at different speeds. In the switchback model, this corresponds to a plateau in the deflection angle at $\theta = \phi$ for $t_2^{\text{or}} < (2f)^{-1} < t_1^{\text{or}}$. The model described by Eqs. (1) and (2) breaks down at very high frequencies, $(2f)^{-1} < t_2^{\text{or}}$, since it predicts no displacement. At first glance, it would seem reasonable to assume that $\theta = \phi$ even at these very high frequencies; the DNA should eventually become oriented along the direction of the stronger electric field, after which time it cannot reorient along the weak field direction. However, this does not appear to be the case in experiments [16].

The switchback model described here can be improved by accounting for additional phenomena, such as the incomplete extension of the chain [23], the displacement of the center of mass during reorientation [21], or adopting a more sophisticated model for the reorientation process. However, these further modifications do not affect the qualitative conclusions of the switchback model, namely a monotonic increase in the deflection angle with frequency

until a plateau regime. We thus chose to investigate the phenomena in more detail using simulations, which allow access to both the microscopic details of the DNA dynamics and the macroscopic behavior manifested in the deflection angle. Our decision is motivated in large part by the success of simulations [19, 37, 38, 42, 43] in describing pulsed field gel electrophoresis in circumstances where theoretical models proved insufficient.

III. BROWNIAN DYNAMICS SIMULATIONS

Our simulations take advantage of a standard simulation algorithm for DNA electrophoresis in post arrays, which is well described by Kim and Doyle [44]. The algorithm implements an inhomogeneous electric field, which is important to capture the DNA movement correctly near the obstacles, especially when there are collisions/holdup during DNA electrophoresis in the post array. The DNA is modeled as a series of N_b beads connected by $N_s = N_b - 1$ springs. The bead positions \mathbf{r}_i are updated by the stochastic force balance

$$\frac{d\mathbf{r}_i}{dt} = -\mu_0\mathbf{E}(\mathbf{r}_i) + \frac{1}{\xi} (\mathbf{F}_i^T + \mathbf{F}_i^B + \mathbf{F}_i^{EV}) \quad (6)$$

where \mathbf{E} is the electric field at position \mathbf{r}_i , ξ is the bead drag coefficient, \mathbf{F}^T is the tension force from the springs connecting two adjacent beads, \mathbf{F}^B is the Brownian force and \mathbf{F}^{EV} is the excluded volume force that accounts for the interaction between beads and an obstacle or the top/bottom boundary of the separation channel. The model does not include any electroosmotic flow. In experiments, it is common to include a polymer that adsorbs to the surface to suppress electroosmotic flow. If there is no suppression, then the dynamics in a post array are quite different [45]. The also model does not include any hydrodynamic interactions, and the interplay between the counterions and the DNA are lumped into the bead electrophoretic mobility, μ_0 . Since the latter mobility is the same as the electrophoretic mobility of the chain as a whole, this model produces an N -independent mobility in free solution. It is known [33, 34] that electrohydrodynamic interactions are critical to capturing the non-monotonic relationship between the electrophoretic mobility and the molecular weight for short DNA in free solution, but the electrophoretic mobility saturates to an N -independent value for DNA longer than a few hundred base pairs [35]. Our prior work, which compared this simulation model to experiments in post arrays under constant electric fields for experimentally relevant ranges of the electric field and molecular weight [29, 31], indi-

cates that the model yields quantitatively realistic predictions of the overall DNA velocity, as well as the microscale distributions (distance between collisions and collision duration) that give rise to the macroscopic behavior [32]. Most likely, the robustness of the model is related to (i) the extensive hydrodynamic screening provided by the posts and (ii) the use of μ_0 as a phenomenological fitting parameter to correctly reproduce the (N -independent) free solution mobility of long DNA. Indeed, similar arguments support the conventional biased reptation models for gel electrophoresis, provided that the free solution mobility is properly defined [19]. It is reasonable to speculate that the remaining quantitative disagreement between the model and experiments is due to electrohydrodynamic effects, but there are no simulation data to date to test such a hypothesis.

The details of calculating the forces in Eq. (6), implementing the boundary conditions, and integrating the stochastic differential equation are described elsewhere [30]. The model parameters are also the same as our previous work [30–32], using a maximum spring length $l = 0.5833 \mu\text{m}$, a persistence length [46] of 53 nm and an effective persistence length [47] of 97.652 nm. Most of our simulations use T4 DNA (169 kbp) and λ DNA (48.5 kbp), which are modeled by 126 beads and 37 beads, respectively. We also simulated 1.5λ (55 beads) and 2λ (74 beads). With the aforementioned value of the spring length l , the λ DNA model corresponds to the typical measurement of $21 \mu\text{m}$ the dyed contour length [6] and the T4 DNA contour length corresponds to $73 \mu\text{m}$.

The simulations mimic the electric field protocol used by Zeng *et al.* [16] in their device. The first part of the square wave uses an electric field $\mathbf{E}_1 = -E_0\mathbf{i}_x$, leading to DNA motion in the $+x$ direction. The second part of the square wave uses an electric field $\mathbf{E}_2 = E_0(\mathbf{i}_x - \mathbf{i}_y)$. The net electric field during the second step of the simulation thus has strength $E_2 = \sqrt{2}E_0$ and leads to DNA motion at an angle $\phi = 135^\circ$ relative to the earlier part of the square wave. The normalized electric field is expressed as the bead-spring Péclet number

$$\text{Pe} = \frac{\mu_0 E_0 \xi l}{k_B T} \quad (7)$$

where k_B is Boltzmann’s constant and T is the absolute temperature. Hereafter, unless specified otherwise, all parameters and variables are dimensionless using length l and the bead diffusion time $\xi l^2/k_B T$. If we parameterize the model with experimental data [30], then $\text{Pe} = 1$ corresponds to an electric field around 16 V/cm, dimensionless time $t = 1$ translates to 20 ms, and one unit length is $0.5833 \mu\text{m}$. We will frequently make use of a

dimensionless frequency f , where $f = 1$ is approximately 50 Hz (the inverse bead diffusion time in dimensional units).

The post array consists of an infinitely extended hexagonal array of $1\ \mu\text{m}$ diameter posts with a $3\ \mu\text{m}$ center-to-center distance. The posts span the $4.5\ \mu\text{m}$ height of the separation chamber. The $4.5\ \mu\text{m}$ high chamber is used to reflect channel heights used in separation experiments to increase the signal and to stay within the constraints of deep reactive ion etching of high aspect ratio features. In the simulations, the frequency of the chains colliding with the top/bottom boundary is about 1% of the total time. Before starting the simulation, the DNA is relaxed in free solution for 10^5 time steps with time step $\delta t = 1 \times 10^{-4}$. The DNA is then placed inside the array and further relaxed in the absence of an electric field for another 10^5 time steps (T4 DNA) or 10^4 time steps (λ DNA) with $\delta t = 1 \times 10^{-4}$. This procedure was performed twelve times for each molecular weight to generate the ensemble of initial conditions; the same set of initial conditions but different random seeds were used for each Péclet number and field frequency. We simulated 12 trajectories for each Péclet number and square wave frequency f . The trajectories were terminated when the center-of-mass position reached a dimensionless distance of $y = 2000$. The corresponding dimensional distance of 1.17 mm is close to the 3 to 4 mm distance used in experiments [14, 16].

It is exceedingly difficult to simulate an asymptotically low frequency trajectory, since the time required to simulate each pulse becomes prohibitively expensive. Moreover, the accumulation of round-off errors in such a long simulation leads to error in the deflection angle. These computational considerations motivated our decision to simulate also constant field dynamics under \mathbf{E}_1 or \mathbf{E}_2 . When necessary, we will extract the asymptotic behavior by combining the two constant field simulations into an effective low frequency simulation (i.e., by ignoring the reorientation time). These steady-field simulations again used 12 molecules over a total dimensionless displacement of 2000 starting from the initial configuration used for the DNA prism simulations.

In the data analysis, we define the deflection angle θ relative to the $+x$ -axis, as defined in Eq. (2), such that an angle $\theta = 90^\circ$ corresponds to motion along the time-average electric field and $\theta = 135^\circ$ corresponds to motion along the strong electric field, \mathbf{E}_2 . We chose the latter definition to provide consistency with previous literature in pulsed field gel electrophoresis [19], although other definitions for $\theta = 0$ are equally valid [16, 21]. We also report data for the root-mean-squared fractional extension of the DNA, L_e/L , where L is the contour

length and L_e is the end-to-end distance of the DNA, and the probability p of observing a “plateau switchback”. In a plateau switchback, the net displacement of the DNA center of mass during a given period k of the square wave is parallel to the stronger electric field vector, \mathbf{E}_2 . To account for the stochastic nature of the simulation, we consider any angle $130^\circ < \theta_k < 135^\circ$ as a plateau switchback in the data analysis. If the switchback model is valid, we would expect to observe $p \approx 1$ for $t_2^{\text{or}} < (2f)^{-1} < t_1^{\text{or}}$. Thus, the parameter p allows us to quantitatively connect a plateau (or lack thereof) in the deflection angle to the microscale dynamics.

IV. SIMULATION RESULTS

A. Validity of the switchback model

We begin our discussion by considering the validity of the switchback model using a fixed molecular weight (T4) and electric field ($\text{Pe} = 2$). The T4 DNA contour length $L = 73 \mu\text{m}$ is long compared to the $3 \mu\text{m}$ distance between posts, and the value $\text{Pe} = 2$ ensures that convective motion on the bead-scale is stronger than diffusive motion. One would expect that the switchback model might be valid in this regime, with its accuracy increasing as the molecular weight and Péclet number increase. However, the data for the deflection angle in Fig. 2 shows that the overall behavior mimics the experimental results [16], rather than the predictions of the switchback model. There is a clear maximum in the deflection angle, followed by a decay to $\theta = 90^\circ$. There is also no switching frequency f where plateau switchback behavior $p \approx 1$ occurs. Indeed, the various predictions for the reorientation times in Eqs. (3) and (4) seem to indicate the order of magnitude of the switching frequency corresponding to the onset of the peak in the deflection angle, rather than the onset of a plateau. Finally, the chain stretching, which is constant in the switchback model, exhibits a behavior similar to the deflection angle. The data in Fig. 2 do not support the basic assumptions behind the switchback model.

To understand the particular deviations between the switchback model and the simulation results, it will prove convenient to analyze the dynamics at low, medium and high frequencies separately. Based on the data in Fig. 2, we selected $f = 0.005$ as a low frequency, $f = 0.0143$ as a medium frequency and $f = 0.0896$ as a high frequency. To aid in our discussion, Fig. 3

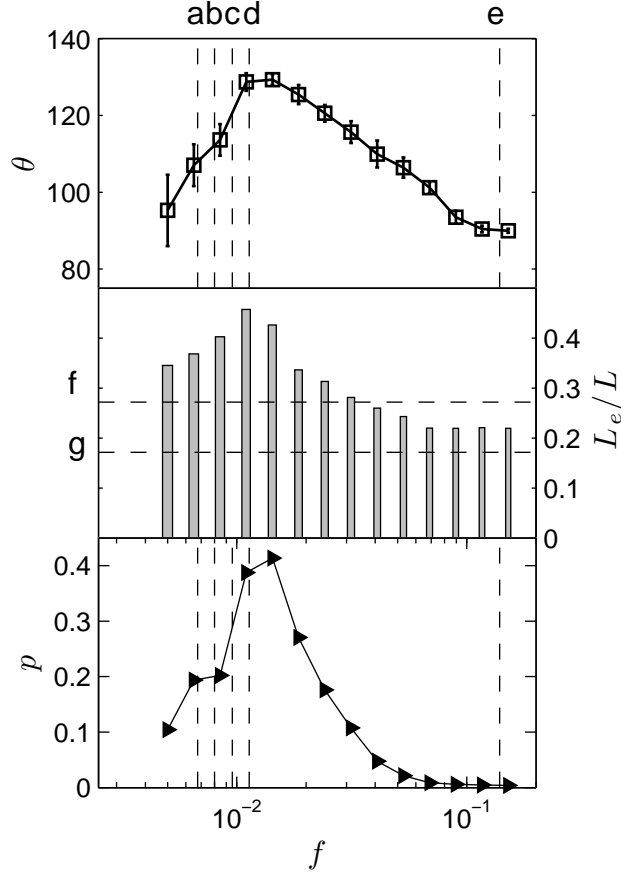


FIG. 2. Plot of the deflection angle θ , root-mean-squared fractional extension, L_e/L , and probability of a “plateau switchback”, p , for T4 DNA as a function of the switching frequency f for $Pe = 2$. There are 14 frequencies simulated, ranging from 0.005 to 0.1514, evenly distributed on the log scale. Each data point represents the average of 12 molecules measured when migrating over a dimensionless distance of 2000 (~ 1.17 mm) in the y -direction. The error bars in the deflection angle correspond to the standard deviation between 12 runs. The dashed lines represents the reorientation frequencies obtained from (a) Eq. (4) at E_1 , (b) Eq. (3) at E_1 , (c) Eq. (4) at E_2 , and (d) Eq. (3) at E_2 , and (e) the confinement frequency. The horizontal dashed lines represent the average stretching for (f) the strong field E_2 and (g) the weak field E_1 obtained from constant field simulations.

shows three representative trajectories obtained at these different frequencies and Fig. 4 shows the corresponding fractional extensions as a function of the cycle number.

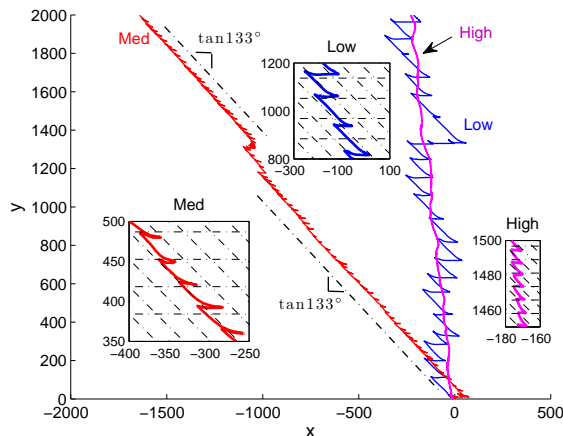


FIG. 3. (color online) Representative trajectories for the DNA center of mass for three different frequencies $f = 0.005$, 0.0143 and 0.0896 , denoted as “Low” (blue), “Med” (red) and “High” (purple), respectively. The corresponding subplots highlight the local details. In the subplots, the dash-dot lines indicate the directions of the two applied electric fields. For the medium frequency trajectory, the two parallel dash-dot lines of slope $\tan 133^\circ$ show the deflection angle during the indicated portion of this trajectory. All of the data correspond to T4 DNA at $Pe = 2$.

1. Low frequencies

By definition, a low frequency for switching the electric field corresponds to a case where the reorientation time is short compared to the total pulse time. As we see in Fig. 3, the corresponding trajectory consists of a clear zig-zag pattern over relatively long distances per pulse. Figure 4A shows that the fractional extension oscillates between an elongated chain (during the collision with a post) and a relaxed conformation (during the motion between posts). The latter dynamics are consistent with the standard models of DNA electrophoresis in a post array under a dc electric field [6, 27, 30–32, 48–50].

However, this low frequency trajectory is not yet truly in the low frequency limit, as we can still observe several instances in Fig. 3 (e.g., near $y = 1300$) where the DNA fails to reorient in the new electric field direction. The failed reorientation is associated with a collapse of the chain, which we can see in Fig. 4A near cycle 15. Note that the configurational impact of these failed reorientation events appear to propagate into subsequent pulses; after the DNA finally turns the corner to start moving on the diagonal direction, it also fails to reorient back to the $+x$ -direction on the next pulse and still retains memory of the

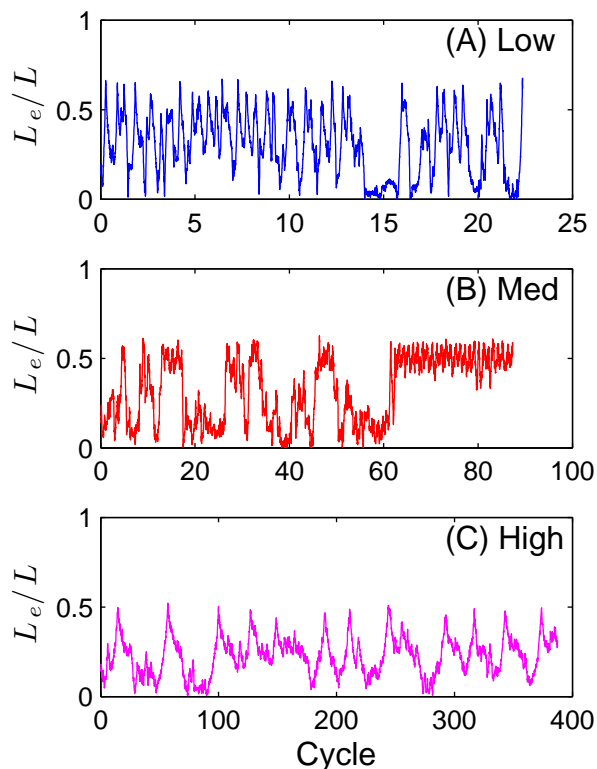


FIG. 4. (color online) Plots of the fractional extension, L_e/L , versus cycle number for the trajectory data in Fig. 3. Note that the number of cycles required to reach $y = 2000$ (the scale for the abscissa on these plots) varies with the switching frequency, f .

collapsed conformation in the previous cycle. This memory effect contrasts sharply with the observations of DNA electrophoresis in a constant electric field [31], which indicate that the DNA loses memory of its previous state during each collision. Once another strong collision event occurs and the chain stretches out, however, the quasi-steady state behavior resumes.

We saw in Fig. 2 that almost no cycles in the low frequency regime correspond to plateau switchback behavior. This result would be expected since the time where the electric field corresponds to \mathbf{E}_1 is much longer than the relaxation time.

2. Medium frequencies

We selected the value for the medium frequency trajectory in Fig. 3 to be the frequency that most closely follows the switchback model for the DNA prism. As we can see in the

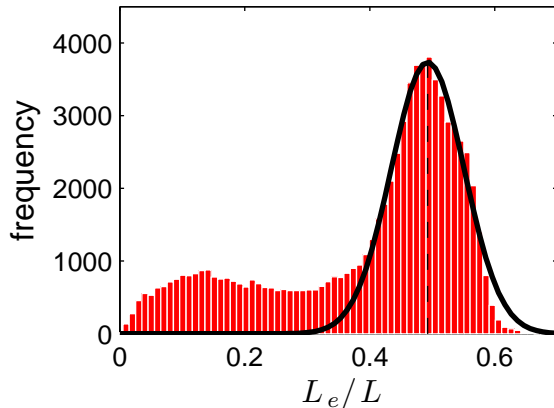


FIG. 5. (color online) Histogram for the rms extension L_e/L at a medium frequency $f = 0.0143$, based on the data from 12 measurements for T4 DNA at $Pe = 2$. The black curve shows a Gaussian fit (mean value = 0.5, standard deviation = 0.057) for the stretched part, corresponding to the states that are described qualitatively by the switchback model.

relevant inset of Fig. 3, over this particular period of time each change in the direction of the electric field is associated with a change in direction of the DNA. Moreover, the reorientation events seen in the inset appear to follow the switchback model in the regime $t_2^{\text{or}} < (2f)^{-1} < t_1^{\text{or}}$; when the field switches to \mathbf{E}_2 , the DNA center-of-mass retraces the path it took under \mathbf{E}_1 and then starts moving along \mathbf{E}_2 . However, when we computed the plateau switchback probability for Fig. 2, we still only reached a value $p \approx 0.4$. This seemingly low value for p results from the arbitrary choice of $130^\circ < \theta_k < 135^\circ$ for determining whether cycle k corresponds to a plateau switchback. In fact, with this criteria, p increases to about 0.7 at the maximum deflection angle θ_{max} at $Pe = 4$, but the corresponding value of θ_{max} only increases from 129° to 131° . As a result, we should consider p as a relative measure of plateau behavior.

The data for the stretching of the DNA provides another possible explanation for the inability to reach the limiting value of $p = 1$ for the plateau switchback, even though the overall deflection angle is close to the predicted plateau value. The switchback model assumes that the DNA is stretched and, in the plateau region, retraces the partial reorientation in the direction of \mathbf{E}_1 during the weaker pulse. We can see in Fig. 2 that, on average, DNA in the medium frequency regime is reasonably well stretched. Indeed, the horizontal lines in Fig. 2 are the averaged extension obtained under a steady electric field \mathbf{E}_1 or \mathbf{E}_2 , both of which lie

below the average extension in the DNA prism at the medium frequency. While the overall extension is less than the full contour length L (the value used in the switchback model), the average extension L_e is almost an order of magnitude higher than the spacing between the posts. However, as we see in Fig. 4, the *instantaneous* extension of the DNA shows large fluctuations. The overall distribution of the stretch at medium frequencies, plotted in Fig. 5, is weighted between 40% to 60% of the full extension, with an almost Gaussian shape. We attribute the time spent in these strongly stretched states to motion that follows the switchback model. However, there is also a very long tail in the distribution towards the lower extensions, with a small peak around 10% extension. These correspond to collapsed states of the chain. Such states can occur during motion in the direction of the stronger electric field, since the time spent under that electric field is longer than the reorientation time. If the electric field switches directions and the chain is in a collapsed state, then the switchback dynamics are not observed. In this way, p links θ and L_e/L , and reveals the similar trend of these two quantities versus f .

For the particular trajectory shown in Fig. 3, there is a small fluctuation in the deflection angle around $y = 1100$. Similar to the low frequency trajectory, it appears that a poorly executed reorientation propagates to subsequent pulses, ultimately leading to a strong fluctuation around $y = 1300$. Afterwards, the trajectory again stabilizes at a well-defined deflection angle that appears to be similar to the original angle. We illustrate this point by the two parallel lines of slope $\tan 133^\circ$. The inverse switching frequency, $(2f)^{-1}$, appears to be slightly shorter than the reorientation time on the strong electric field, leading to a deflection angle slightly less than the maximum value of 135° . The recovery of the steady-state deflection angle after $y = 1300$ is accompanied by the strong stretching after cycle 60 in Fig. 4B.

The microscopic details discussed above unveil the important relationship between p and θ_{\max} . According to the switchback model, the θ - f curve will reach its maximum θ_{\max} when the duration time $(2f)^{-1}$ exceeds the reorientation time t_1^{or} . However, because of the existence of “non-plateau switchback”, indicated by the trajectory detail in Fig. 3 as well as the plateau switchback values $p < 1$ in Fig. 2, the deflection angle θ at the frequency $(2t_1^{\text{or}})^{-1}$ is less than the value predicted by the model. Rather, the data in Fig. 2 indicate that the maximum in the deflection angle should occur at a frequency slightly larger than $(2t_2^{\text{or}})^{-1}$.

This discrepancy between the switchback model predictions for a tight porous medium and our simulations in somewhat sparse post array is explained by considering the extension of the DNA when the field changes direction. In the switchback model, the DNA is always extended and the plateau occurs for $(2f)^{-1} \geq t_1^{\text{or}}$. In the model, the stretched DNA will retrace some of the path in the direction of \mathbf{E}_1 during the weak pulse, but that retracing is undone once the field switches back to the stronger pulse \mathbf{E}_2 . However, these switchback dynamics are only valid for a strongly stretched chain. If the DNA spends too much time in the post array under the stronger pulse \mathbf{E}_2 , it is likely that the DNA will start to relax and exhibit the cycles of collision and translation that characterize its dynamics in a post array under a constant electric field [31, 32]. If the DNA is extended when the field switches from \mathbf{E}_2 to \mathbf{E}_1 , even if the DNA collapsed and underwent a rope-over-pulley collision at some point under \mathbf{E}_2 , then we would still expect to observe plateau switchback behavior since the net displacement of the DNA is only in the direction of \mathbf{E}_2 . However, if the DNA is relaxed or engaged with one (or more) posts when the field switches back to \mathbf{E}_1 , we would not expect to observe switchback behavior because the dynamics under \mathbf{E}_1 no longer correspond to “turning the corner.” There are several instances of such failed reorientation events in the trajectories of Fig. 3, which are correlated with the collapsed states in Fig. 4. The probability that the chain relaxes and thus destroys the switchback on the next pulse increases with the time, $(2f)^{-1} - t_2^{\text{or}}$, available for electrophoresis through the post array after reorientation. As a result, although the switchback model predicts the onset of the plateau at $(2t_1^{\text{or}})^{-1}$, the possibility for the chain to relax while moving under \mathbf{E}_2 implies that θ_{max} should be reached closer to the frequency $(2t_2^{\text{or}})^{-1}$.

3. High frequencies

The high frequency trajectory in Fig. 3, as well as the decreasing deflection angle in Fig. 2, are not predicted by the switchback model. The high frequency behavior corresponds to the case where the frequency is faster than either of the reorientation times. At first glance, the high frequency behavior looks like an almost straight trajectory, with a deflection angle of $\theta = 94^\circ$. However, as we see in the high frequency inset of Fig. 3, there is still a clear zig-zag behavior. Moreover, Fig. 4C shows that the chain remains in a fairly compact conformation. Overall, Fig. 2 shows that both the probability of being in a stretched state

and the probability of executing a plateau switchback decrease with the switching frequency in the high frequency regime. These two features of the dynamics are related; if the DNA cannot adopt a stretched conformation, then it cannot follow the switchback dynamics.

The high frequency behavior is interesting from a physical standpoint. The theories for pulsed field gel electrophoresis [51] predict that the high frequency behavior for a long chain should correspond to an effective field regime. If the DNA is undergoing reptation, then the chain will eventually become oriented in the direction of the stronger electric field. When the electric field changes direction, it does not lead to reorientation because the duration of the new electric field is too short. Rather, there should be some backtracking of the head of the chain into the reptation tube. When the electric field returns to the stronger direction, the head of the chain needs to extend back out of the reptation tube and, possibly, select a new direction [51]. The net effect is that the chain has an effective mobility that is akin to biased reptation, albeit with a renormalized field that accounts for the frequent switching of the electric field.

We did not observe an effective field regime because the high porosity of the post array suppresses the biased reptation behavior. Indeed, this suppression is critical to separations of long DNA in dc electric fields in a post array [6]. Since the T4 DNA can coil inside the pores of the post array, a very high frequency electric field leads to the DNA “bouncing” between posts. The duration of the electric field in a given direction is shorter than the unraveling time for the coiled DNA [49], so the chain remains primarily in a relaxed conformation. We can make a crude approximation for the onset of a high frequency as the nominal time for convection across a pore. In the case of a post array where the obstacles are separated by a distance a , the dimensionless time is

$$t_c = \frac{(a/l)}{\text{Pe}} \quad (8)$$

The corresponding frequency $f_c = 1/2t_c$, plotted in Fig. 2 as line (e), agrees well with this approximation. For the particular electric field and hexagonal post arrays used in our simulations, the deflection angle is $\theta \approx 90^\circ$ for $f \gtrsim f_c$.

Similar to what we saw in the medium frequency case, the failure to observe plateau switchback behavior can also be described from the perspective of the plateau switchback probability, p . After θ achieves its maximum value θ_{\max} , the reason we do not observe plateau switchback behavior for high f is not the extra time for collision or relaxation, since

there is not enough time for DNA to reorient to either direction, $t_1^{\text{or}} > t_2^{\text{or}} > (2f)^{-1}$. Rather, the plateau switchback behavior is suppressed because there is not enough time for DNA to be stretched and form the shape assumed in the switchback model. As f keeps increasing, once the DNA deviates from the stretched mode and becomes coiled, it becomes harder for DNA to restore to the plateau switchback mode. Thus p decrease with f as shown in Fig. 2 on the downhill side. The extreme case will be at f_c , when no stretching is possible for such a high frequency, and p approaches zero.

B. Electric field and molecular weight

Our results at fixed Pe and molecular weight in Fig. 2 suggest two generic features of the dependence of the deflection angle on the switching frequency. First, the frequency corresponding to the peak in the deflection angle is correlated, but not exactly equal to, the reorientation time of the chain given by the simple models in Eq. (3) or Eq. (4), with the reorientation time t_2^{or} in the stronger field being the best predictor for the location of θ_{max} . Thus, we would expect the frequency f_{max} corresponding to the peak in the deflection angle to shift to higher frequencies as we either increase the Péclet number or decrease the molecular weight. Second, the frequency corresponding to a size-independent deflection angle is approximately given by the confinement time in Eq. (8). The corresponding frequency f_c increases as we increase the Péclet number.

The latter observations are sufficient to understand how the θ - f curves shift as a function of electric field and molecular weight. Figure 6 shows how the deflection angle depends on frequency for both λ DNA (37 beads) and T4 DNA (126 beads) at $\text{Pe} = 2$ and $\text{Pe} = 4$. For a fixed molecular weight, the peak frequency f_{max} increases with Péclet number, in accord with our reasoning in the previous paragraph. Likewise, for a fixed Péclet number, the peak frequency f_{max} decreases with increasing molecular weight. The location of the confinement frequency f_c also agrees with our argument, increasing with Péclet number.

The peak in the T4 DNA deflection angle, $\theta = 128.5^\circ$ ($\text{Pe} = 2$) or 131° ($\text{Pe} = 4$), corresponds to net motion almost along the direction of $-\mathbf{E}_2$ at both Péclet numbers. In contrast, the peak in the deflection angles for the λ DNA are at much lower angles. The reduced deflection angle for λ DNA is due to weak stretching in this relatively porous post array. Previous simulations and experiments [29, 31, 32] of λ DNA electrophoresis

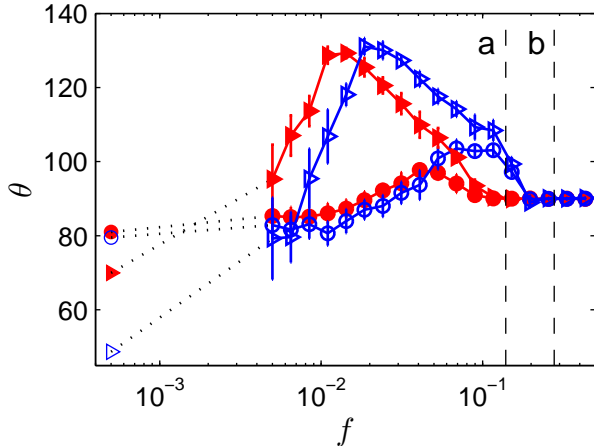


FIG. 6. (color online) Deflection angle as a function of frequency for T4 DNA (triangles) and λ DNA (circles) at $Pe = 2$ (solid symbols) and $Pe = 4$ (open symbols). Each data point represents the average of 12 molecules measured when migrating over a dimensionless distance of 2000 (~ 1.17 mm) in the y -direction. The error bars correspond to the standard deviation between 12 runs. The markers on the far left denote the deflection angle for “zero-frequency” case, where θ is only related to the velocities of DNA under the a constant strong or weak electric field. The dashed lines connecting the zero-frequency deflection angles are only to guide the eye, and the value of f corresponding to the zero-frequency result on the semilog plot is arbitrary and chosen for convenience. The vertical dotted lines represents the inverse confinement time (i.e., the frequency f_c) for $Pe = 2$ (line a) and $Pe = 4$ (line b).

in this sparse post array indicate that there is sufficient space inside the array for λ DNA to relax inside the pores. As a result, we would not expect the switchback model to be a good description for the dynamics of such a small DNA molecule (relative to the pore spacing) in the DNA prism protocol, especially under weak electric fields. When the Péclet number increases to $Pe = 4$, corresponding to an electric field $E_0 \approx 64$ V/cm, the maximum deflection angle for λ DNA becomes appreciable but still rests well below the switchback model’s prediction of $\theta = 135^\circ$. In other words, for a given size DNA, a larger pore size will lead to more DNA relaxation. Therefore, the deflection angle and the average fractional extension will be smaller. For the same pore size, the bigger DNA has the larger maximum deflection angle. The relationship role of relaxation in the pores explains the increase in θ_{\max} of λ DNA in Fig. 6 from $Pe = 2$ to 4, where the stretching of DNA is increased with

higher Pe. The connection between pore size and separation is also evident in experiments in the DNA prism [21], where the smaller pore sizes give rise to larger deflection angles.

The different behavior of small and large DNA molecules in a post array under the DNA prism protocol provides the efficient method to filter DNA we saw at the outset in Fig. 1. Figure 6 shows that there exists a frequency at which the larger T4 DNA is strongly deflected in the DNA prism, whereas the λ DNA tends to move at an angle $\theta \approx 90^\circ$. We determined a good choice for frequency for Fig. 1 from the data in Fig. 6 by choosing the peak in the θ - f curve for T4 DNA. This generic strategy was previously used as one component of an integrated genome scanning device [15], where the larger DNA are shunted to the analysis portion of the device while the small DNA contaminants are removed by the DNA prism.

In addition to scanning the frequency space in Fig. 6, we also computed the asymptotic values of the deflection angle that we would expect to observe at zero frequency. Here, we would expect the reorientation time to play an asymptotically small role and can be ignored in Eq. (1). We measured the quantity $\mu_{i,j}\mathbf{E}_j$ using simulations under a constant electric field \mathbf{E}_j with $j = 1,2$ for $i = \text{T4 DNA or } \lambda \text{ DNA}$, and then computed the expected deflection angle θ from Eqs. (1) and (2). As Fig. 6 is a semilog plot, we simply placed these results for $f \rightarrow 0$ at some arbitrary small value of f and used dotted lines to connect the asymptotic results to the relevant θ - f curve.

The zero-frequency results point out an important role of the post array geometry. Although $|\mathbf{E}_2| = \sqrt{2}|\mathbf{E}_1|$ and μ_0 is independent of molecular weight, we did not find that $\mu_{i,2}|\mathbf{E}_2| = \sqrt{2}\mu_{i,1}|\mathbf{E}_1|$. Rather, the steady electric field simulations yielded the mobility ratios $\mu_{\text{T4},2}/\mu_{\text{T4},1} = 1.04$ (Pe = 2) or 0.75 (Pe = 4) and $\mu_{\lambda,2}/\mu_{\lambda,1} = 1.22$ (Pe = 2) or 1.19 (Pe = 4). These ratios reflect the microstructure of the post array, which is characterized by the lattice vectors of a hexagonal array. In principle, it is possible to separate these DNA by size using a very low frequency DNA prism. Likewise, we would expect that separations should be possible in a very low frequency DNA prism using colloidal crystals, provided that the crystal can be constructed without any defects. Obviously, a low frequency separation is not a practical approach since it would require an extremely large device. In the case of colloidal crystals, the problem is compounded by the difficulty in fabricating large scale, defect free crystals [52].

It is interesting also to consider the behavior of a zero-frequency DNA prism if the protocol was implemented in an agarose gel. An agarose gel is disordered, so it can be

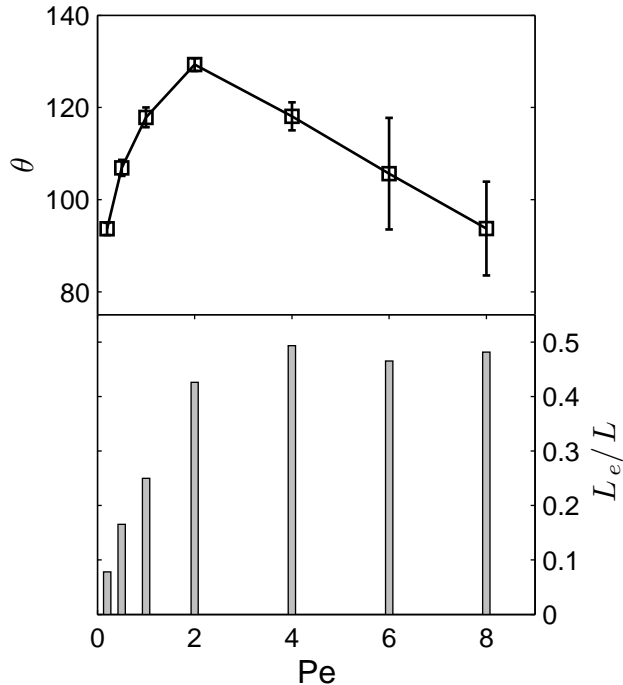


FIG. 7. Deflection angle and fractional extension as a function of Péclet number for T4 DNA at a switching frequency $f = 0.0143$. Each data point represents the average of 12 molecules measured when migrating over a dimensionless distance of 2000 (~ 1.17 mm) on y direction. The error bars correspond to the standard deviation from the 12 measurements.

modeled as an isotropic medium. In the biased reptation without orientation regime [19], the electrophoretic mobility is $\mu \sim L^{-1}E^0$. As a result, we would expect $\mu_{i,1} = \mu_{i,2}$, independent of the applied electric field. Therefore, all of the DNA would move in the direction of the average electric field direction. However, if a DNA prism in an agarose gel used a strong enough field to enter the biased reptation with orientation regime [19], the electrophoretic mobility has the scaling $\mu \sim L^0E^1$. While we now have $\mu_{i,1} \neq \mu_{i,2}$, the ratio $\mu_{i,1}/\mu_{i,2}$ is independent of molecular weight. As a result, although the deflection angle at zero frequency will depend on the electric field E_0 , all of the DNA will adopt the same deflection angle for a given value of E_0 . Thus, although one can implement a low-frequency DNA prism separation in a sparse, ordered medium, such as a post array, similar separations cannot be achieved in a dense, disordered medium.

We have also explored the role of the electric field in more depth. Figure 7 shows how

the deflection angle changes for T4 DNA if we fix the frequency at the value $f = 0.0143$ corresponding to the peak in the deflection angle in Fig. 2. To facilitate our explanation of this figure, let us clarify that the frequency corresponding to the maximum in the deflection angle for a fixed molecular weight is a function of Péclet number, $f_{\max} = f_{\max}(\text{Pe})$. Thus, the data in Fig. 7 correspond to a frequency $f \approx f_{\max}(\text{Pe} = 2)$. Since we already confirmed our intuition that f_{\max} increases with Pe in Fig. 6, the data in Fig. 7 for $\text{Pe} > 2$ correspond to cases where $f < f_{\max}(\text{Pe})$. From a physical standpoint, we are now operating in the regime on the ascent towards the maximum deflection angle at a given Péclet number. (In other words, we are operating somewhere to the left of the peak in the version of Fig. 2 for a given Péclet number.) Moreover, as the Péclet number increases at fixed f , the ratio $f/f_{\max}(\text{Pe})$ gets smaller. As a result, these higher Péclet number simulations are operating even further from the frequency corresponding to the maximum deflection angle. This reasoning explains the decrease in the deflection angle in Fig. 7 for Pe increases past the peak value at $\text{Pe} = 2$.

A similar logic applies to the increase in the deflection angle as a function of Péclet number for $\text{Pe} < 2$. Here, we are operating in a regime where $f > f_{\max}(\text{Pe})$. As a result, we are in the region of a curve similar to Fig. 2, albeit for a different Pe, where the deflection angle is approaching the size-independent value at the inverse confinement time. Again using the reasonable assumption that $f_{\max}(\text{Pe})$ increases with Pe, the smaller values of Pe in Fig. 7 correspond to frequencies that are closer to the inverse confinement time. Thus, the deflection angle again decays as the Péclet number is decreased from $\text{Pe} = 2$.

The stretching data in Fig. 7 do not exhibit the same correlation with the deflection angle that we observed in Fig. 2. At the higher Péclet numbers, the stretching as a function of Péclet number at a fixed frequency results from the competition between two different effects. All other things being equal, the stretching should increase with Péclet number because the electric force acting on a hooked chain increases. However, we also know from Fig. 2 that the stretching increases when the frequency is closest to the reorientation frequency. This competition between effects is apparent in the high Péclet number data in Fig. 7; the increased force acting to stretch the chain appears to be almost offset by the decreasing ratio $f/f_{\max}(\text{Pe}) < 1$. Our conjecture is supported by the data in Fig. 8, which shows that the stretching at $\text{Pe} = 4$ is generally larger than that of $\text{Pe} = 2$, but that their maxima lie at different frequencies. The particular data in Fig. 7 correspond to $f = 0.0143$, where the stretching at the two different Péclet numbers in Fig. 8 is roughly equivalent. At the lower

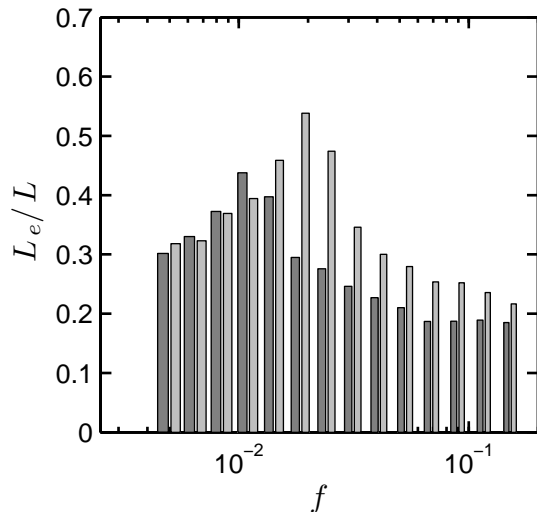


FIG. 8. The fractional extension, L_e/L , as a function of the switching frequency, f , for T4 DNA at two different Péclet numbers, $Pe = 2$ (dark gray) and $Pe = 4$ (light gray).

Péclet numbers, these two effects are synergistic. As the Péclet number increases from a small value, the electric force acting on the chain increases and the ratio $f/f_{\max}(Pe) > 1$ decreases towards the optimal value of unity. The synergy between the role of the overall electric field strength and the switching frequency leads to a monotonic increase in the stretching with increasing Péclet number for $Pe < 2$.

V. CONNECTION TO EXPERIMENTAL DATA

Thus far, we have focused primarily on elucidating the basic physics of DNA electrophoresis in a DNA prism. In doing so, we have explained the experimentally observed [16] non-monotonic behavior of the deflection angle as a function of frequency. So long as the DNA can span many pores, which is the case for a long molecule in a strong electric field, then the deflection angle increases monotonically with the switching frequency for small values of f . However, in contrast to the prediction of the switchback model, the deflection angle eventually reaches a molecular weight-independent deflection angle when the frequency exceeds the confinement frequency given by half of the inverse of Eq. (8). For the particular electric field program we used here [16], the maximum in the deflection angle is $\theta_{\max} = 135^\circ$ and the value of the high frequency deflection angle is $\theta = 90^\circ$. As a result, the deflection angle must

exhibit a maximum. If the DNA does not span many pores, even at a medium frequency where switchback behavior should be manifest, then the maximum deflection angle is $\theta_{\max} < 135^\circ$ because the reptation behavior required by the switchback model no longer occurs.

In addition to capturing the non-monotonicity of the experimental θ - f data, the overall trends that we observed as a function of molecular weight and Péclet number agree well with experiments [16]. We focus first on experimental data for 10 kbp and 20 kbp DNA at 70 V/cm and 169 V/cm in a colloidal crystal of 330 nm diameter colloids, which appear as Fig. 3 of Ref. [16]. These experimental data show an increase in f_{\max} with increasing electric field and a decrease in f_{\max} with increasing molecular weight. We previously saw these trends in Fig. 6.

We can also understand the relationship between the electric field and the switching frequency required to operate the DNA prism. In the original experiments in a DNA prism, Huang *et al.* [14] suggested that the best separations occur at a low electric field/small switching frequency or at a high electric field/fast switching frequency. We know from our simulations that the θ - f curve shifts to the right as the Péclet number increases. Thus, in order to maintain a frequency near f_{\max} for one of the species, the frequency also needs to increase. Thus, the relationships between the deflection angle and the switching frequency seen in our simulation data explain this rule of thumb.

The generic shape of the θ - f curves, sketched in Fig. 9, also explain the band shifting behavior observed in experiments in the DNA prism using a post array [14]. These experiments showed that while only three of a possible four bands are resolved at one frequency, an increase in the frequency (at fixed electric field) resolves all four bands while “shifting” the deflection angle of the larger bands to smaller deflection angles. The latter behavior is inconsistent with the switchback model, since the deflection angles are monotonic as a function of switching frequency. As we illustrate in Fig. 9A, the band shifting phenomenon is explained by the trends in our simulation data. The frequency at which the deflection angle becomes sensible decreases with increasing molecular weight. Thus, at a low frequency f_1 , it is possible that the two smallest DNA in the experiments [14] have very small deflection angles while the two largest DNA are close to their maximum deflection angles. In order to resolve all four peaks, Huang *et al.* [14] selected a faster switching frequency f_2 so that the deflection angle of at least one of the smaller DNA becomes sensible. However, as illustrated in Fig. 9A, if the original frequency $f_1 \approx f_{\max}$ for the larger DNA, then these DNA are on the

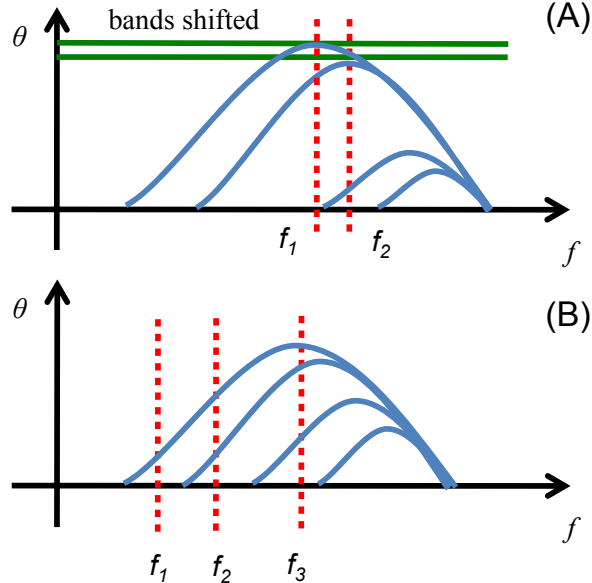


FIG. 9. (color online) Schematic θ - f curves explaining various experimental phenomena in DNA prism experiments in (A) a post array [14] and (B) a colloidal crystal [16].

downward slope of their θ - f behavior at f_2 . Thus, the trends emerging from our simulation data predict that the bands for the larger DNA shift to a lower deflection angle, consistent with the band shifting observed in experiments.

In related experiments using a colloidal crystal and a mixture of four different DNA sizes, Zeng *et al.* [16] observed that the number of resolved bands increased from two to three to four as the switching frequency increased. The θ - f curve in Fig. 9B explains the latter behavior, again taking advantage of the observations that shorter DNA achieve a sensible deflection angle at higher switching frequencies. In the latter experiments, it appears that all of the frequencies correspond to $f \leq f_{\max}$, as the deflection angles still increase monotonically as a function of switching frequency. We propose that the relatively flat behavior of the deflection at low frequencies for the smaller DNA in Fig. 6, which contrasts with the prediction of the switchback model, is the origin for the appearance of additional bands as the frequency increases.

To provide further support for our qualitative explanation of the physics underlying the experiments, we also simulated the θ - f curve for DNA of sizes 1.5λ and 2λ at $Pe = 4$. Figure 10 plots these data along with the relevant curves for T4 and λ DNA from Fig. 6. The similarity between the simulation data and our qualitative sketch in Fig. 9 is apparent.

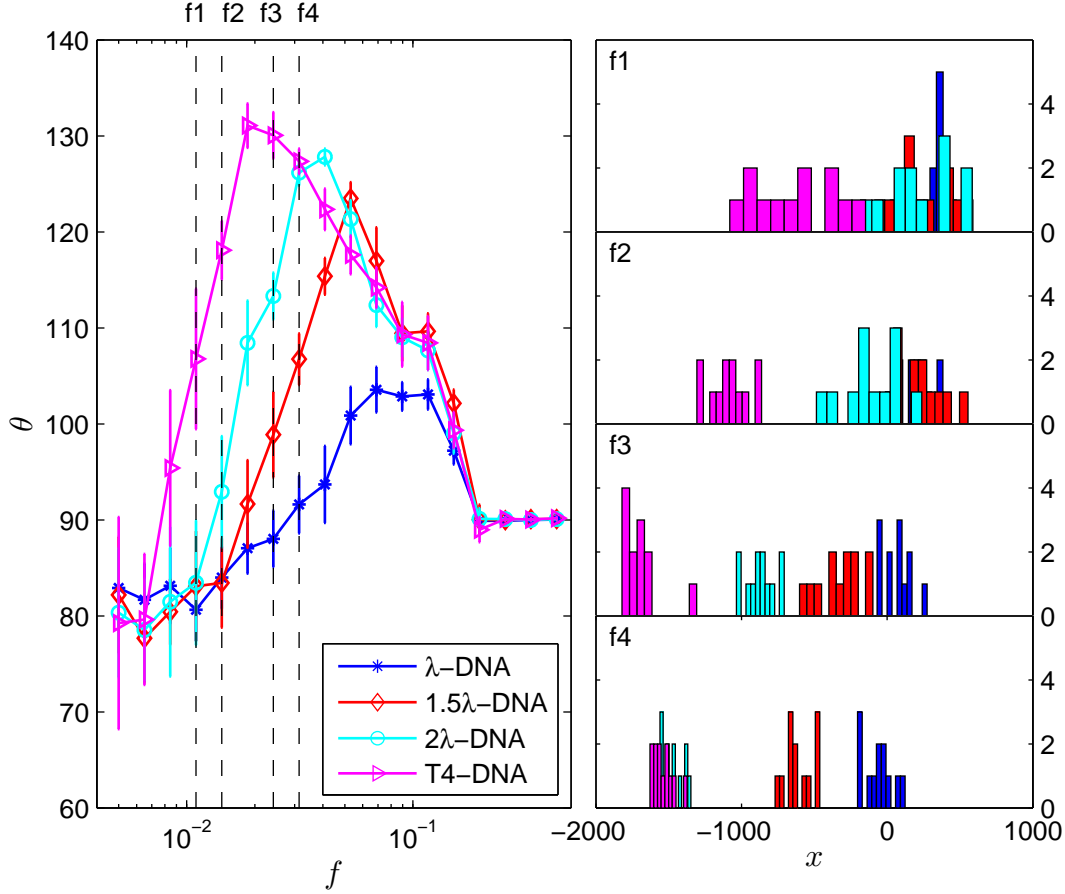


FIG. 10. (color online) The deflection angle θ versus the switching frequency f (on the left) for different size DNA at $Pe = 4$. The right panel contains histograms for the outlet positions of these four species at four different frequencies, where $f_1 = 0.0143$, $f_2 = 0.0186$, $f_3 = 0.0241$, and $f_4 = 0.0314$ (from top to bottom).

In addition to the depicting the θ - f behavior, Fig. 10 also plots the electropherograms that would be obtained at the outlet of this DNA prism for four different frequencies. Although these histograms only contain the 12 DNA from the simulations, they reproduce all of the experimentally observed behavior described above. As we increase from f_1 to f_2 to f_3 , each increment enables an additional band of DNA to be resolved at the outlet. However, when we further increase the frequency to f_4 , the T4 is “band shifted” to such an extent that it can no longer be resolved from the 2λ band.

VI. CONCLUSIONS

In this paper, we have shown the shortcomings of the switchback model when applied to the DNA prism. There are three major differences between the switchback model and our simulation results. First, the deflection angle θ does not reach its maximum at a frequency corresponding to the inverse of the reorientation time in the weaker field, $(2t_1^{\text{or}})^{-1}$. Second, for frequencies $f > (2t_1^{\text{or}})^{-1}$, the deflection angle keeps rising instead of forming a plateau. Third, θ decreases with increasing f after θ passes through its peak value, θ_{max} , eventually reaching a deflection angle corresponding to the direction of the time-averaged electric field.

While the simulation results do not agree with the switchback model, they are consistent with experimental data [16]. By analyzing the microscopic details of the transport process, we showed that deviations from “plateau switchback” behavior leads to reduced values of the deflection angle for $(2t_1^{\text{or}})^{-1}$. When f keeps increasing, the probability p of observing plateau switchback behavior increases, leading to concomitant increases in θ and the fractional extension, L_e/L . However, we do not observe perfect switchback behavior in a post array because the DNA can still relax in the strong field direction. Moreover, when f becomes large, there is not enough time for DNA to stretch and restore the plateau switchback mode. Thus, after the deflection angle reaches a peak corresponding to the most “switchback-like” dynamics, the probability of observing plateau switchback behavior decreases with increasing frequency, resulting in the downhill side of θ - f curve. The extreme case is for $f > f_C$, when the DNA, even for rather long molecules, will hardly be stretched and be confined between two adjacent obstacles like a bouncing ball.

Based on this understanding, we were able to make simple qualitative predictions of θ - f curve behavior for different DNA size (L) and electric field strength (Pe). For the same Pe, shorter DNA will attain its maximum at higher f than that for longer DNA and, generally, θ_{max} of short DNA will be smaller than that of long DNA. For the same DNA, increasing Pe will shift the θ - f curve to right. These overall trends allow us to explain most of the interesting phenomena observed in experiments.

We have focused here on the phenomenology underlying the separations in the DNA prism device. While our data proved sufficient to explain the experimental trends, additional simulations as a function of Péclet number and molecular weight are required to establish a complete description of the relationship between the frequency and deflection angle. We are

confident that such simulations would provide a more detailed phenomenological description of the separation, but it remains to be seen whether meaningful scaling results will emerge. Our results also leave open questions related to the pore structure, since we focused exclusively on a single, perfectly periodic post array geometry. The pore spacing should be important for shorter DNA, which is apparent in our data for λ DNA, but its effect should eventually saturate to some appropriate renormalization of the fractional extension as the DNA becomes large compared to the pore size. Even more rich physics should emerge in the three-dimensional pore spaces provided by colloidal crystals [16, 21], especially if we further consider the disorder and defects [22] in self-assembled media. While we have made the first inroads into explaining the physics behind the DNA prism, phase space for these separations is large. In addition to a more complete description of the process, further simulations may also reveal more efficient locations in the phase space for separations. We expect that the basic understanding obtained here will form the basis for both designing more efficient devices and deepening our physical understanding.

ACKNOWLEDGMENTS

This work was supported by NIH Grant No. R21-GM103409 and was carried out in part using computing resources at the University of Minnesota Supercomputing Institute.

-
- [1] J. O. Tegenfeldt, C. Prinz, H. Cao, L. R. Huang, R. H. Austin, S. Y. Chou, E. C. Cox, and J. C. Sturm, *Anal. Bioanal. Chem.* **378**, 1678 (2004).
 - [2] J. Han, J. Fu, and R. B. Schoch, *Lab Chip* **8**, 23 (2008).
 - [3] G. B. Salieb-Beugelaar, K. D. Dorfman, A. van den Berg, and J. C. T. Eijkel, *Lab Chip* **9**, 2508 (2009).
 - [4] S. L. Levy and H. G. Craighead, *Chem. Soc. Rev.* **39**, 1133 (2010).
 - [5] N. Kaji, K. Okamoto, M. Tokeshi, and Y. Baba, *Chem. Soc. Rev.* **39**, 948 (2010).
 - [6] K. D. Dorfman, *Rev. Mod. Phys.* **82**, 2903 (2010).
 - [7] K. D. Dorfman, S. B. King, D. W. Olson, J. D. P. Thomas, and D. R. Tree, *Chem. Rev.* (submitted).

- [8] C. F. Chou, O. Bakajin, S. W. P. Turner, T. A. J. Duke, S. S. Chan, E. C. Cox, H. G. Craighead, and R. H. Austin, Proc. Natl. Acad. Sci. U.S.A. **96**, 13762 (1999).
- [9] M. Cabodi, Y. F. Chen, S. W. P. Turner, H. G. Craighead, and R. H. Austin, Electrophoresis **23**, 3496 (2002).
- [10] L. R. Huang, P. Silberzan, J. O. Tegenfeldt, E. C. Cox, J. C. Sturm, R. H. Austin, and H. G. Craighead, Phys. Rev. Lett. **89**, 178301 (2002).
- [11] L. R. Huang, E. C. Cox, R. H. Austin, and J. C. Sturm, Anal. Chem. **75**, 6963 (2003).
- [12] L. R. Huang, E. C. Cox, R. H. Austin, and J. C. Sturm, Science **304**, 987 (2004).
- [13] J. Fu, R. B. Schoch, A. L. Stevens, S. R. Tannenbaum, and J. Han, Nat. Nanotechnol. **2**, 121 (2007).
- [14] L. R. Huang, J. O. Tegenfeldt, J. J. Kraeft, J. C. Sturm, R. H. Austin, and E. C. Cox, Nat. Biotechnol. **20**, 1048 (2002).
- [15] R. H. Meltzer, J. R. Krogmeier, L. W. Kwok, R. Allen, B. Crane, J. W. Griffis, L. Knaian, N. Kojanian, G. Malkin, M. K. Nahas, V. Papkov, S. Shaikh, K. Vyavahare, Q. Zhong, Y. Zhou, J. W. Larson, and R. Gilmanishin, Lab Chip **11**, 863 (2011).
- [16] Y. Zeng, M. He, and D. J. Harrison, Angew. Chem. Int. Edit. **47**, 6388 (2008).
- [17] L. R. Huang, J. O. Tegenfeldt, J. J. Kraeft, J. C. Sturm, R. H. Austin, E. C. Cox, "Generation of large-area tunable uniform electric fields in microfluidic arrays for rapid DNA separation." In *Electron Devices Meeting, 2001. IEDM Technical Digest. International*, IEEE, 2001; pp. 363-366.
- [18] S. M. Clark, E. Lai, B. W. Birren, and L. Hood, Science **241**, 1203 (1988).
- [19] J.-L. Viovy, Rev. Mod. Phys. **72**, 813 (2000).
- [20] O. Bakajin, T. A. J. Duke, J. Tegenfeldt, C.-F. Chou, S. S. Chan, R. H. Austin, and E. C. Cox, Anal. Chem. **73**, 6053 (2001).
- [21] N. Nazemifard, S. Bhattacharjee, J. H. Masliyah, and D. J. Harrison, Angew. Chem. Int. Edit. **49**, 3326 (2010).
- [22] N. Nazemifard, L. Wang, W. Ye, S. Bhattacharjee, J. H. Masliyah, and D. J. Harrison, Lab Chip **12**, 146 (2012).
- [23] T. A. J. Duke, R. H. Austin, E. C. Cox, and S. S. Chan, Electrophoresis **17**, 1075 (1996).
- [24] J. M. Deutsch, Science **240**, 922 (1988).
- [25] J. M. Deutsch and T. L. Madden, J. Chem. Phys. **90**, 2476 (1989).

- [26] P. D. Patel and E. S. G. Shaqfeh, *J. Chem. Phys.* **118**, 2941 (2003).
- [27] A. Mohan and P. S. Doyle, *Macromolecules* **40**, 8794 (2007).
- [28] A. Mohan and P. S. Doyle, *Phys. Rev. E* **76**, 040903(R) (2007).
- [29] J. Ou, J. Cho, D. W. Olson, and K. D. Dorfman, *Phys. Rev. E* **79**, 061904 (2009).
- [30] J. Cho and K. D. Dorfman, *J. Chromatogr. A* **1217**, 5522 (2010).
- [31] D. W. Olson, J. Ou, M. Tian, and K. D. Dorfman, *Electrophoresis* **32**, 573 (2011).
- [32] D. W. Olson, S. Dutta, N. Laachi, M. Tian, and K. D. Dorfman, *Electrophoresis* **32**, 581 (2011).
- [33] K. Grass, U. Bohme, U. Scheler, H. Cottet, and C. Holm, *Phys. Rev. Lett.* **100**, 096104 (2008).
- [34] T. N. Schendruk, O. A. Hickey, G. W. Slater and J. L. Harden, *Curr. Opin. Colloid Interface Sci.* **17**, 74 (2012).
- [35] N. C. Stellwagen, C. Gelfi and P. G. Righetti, *Biopolymers* **42**, 687 (1997).
- [36] E. M. Southern, R. Anand, W. R. A. Brown, and D. S. Fletcher, *Nucleic Acids Res.* **15**, 5925 (1987).
- [37] J. Noolandi, G. W. Slater, H. A. Lim, and J.-L. Viovy, *Science* **243**, 1456 (1989).
- [38] B. H. Zimm, *J. Chem. Phys.* **94**, 2187 (1991).
- [39] J. M. Deutsch, *Phys. Rev. Lett.* **59**, 1255 (1987).
- [40] D. Long and J.-L. Viovy, *Physica A* **244**, 238 (1997).
- [41] G. W. Slater and J. Noolandi, *Electrophoresis* **10**, 413 (1989).
- [42] M. S. Hutson, G. Holzwarth, T. Duke, and J.-L. Viovy, *Biopolymers* **35**, 297 (1995).
- [43] L. M. Neitzey, G. Holzwarth, T. Duke, and J.-L. Viovy, *Biopolymers* **35**, 307 (1995).
- [44] J. M. Kim and P. S. Doyle, *J. Chem. Phys.* **125**, 074906 (2006).
- [45] N. Kaji, A. Oki, R. Ogawa, Y. Takamura, Y. Nishimoto, H. Nakanishi, Y. Horiike, M. Tokeshi, and Y. Baba, *Isr. J. Chem.* **47**, 161 (2007).
- [46] C. Bustamante, J. F. Marko, E. D. Siggia, and S. Smith, *Science* **265**, 1599 (1994).
- [47] P. T. Underhill and P. S. Doyle, *J. Non-Newtonian Fluid Mech.* **122**, 3 (2004).
- [48] W. D. Volkmuth, T. Duke, M. C. Wu, R. H. Austin, and A. Szabo, *Phys. Rev. Lett.* **72**, 2117 (1994).
- [49] G. I. Nixon and G. W. Slater, *Phys. Rev. E* **50**, 5033 (1994).
- [50] N. Minc, J.-L. Viovy, and K. D. Dorfman, *Phys. Rev. Lett.* **94**, 198105 (2005).
- [51] J.-L. Viovy, *Electrophoresis* **10**, 429 (1989).

- [52] D. J. Norris, E. G. Arlinghaus, L. Meng, R. Heiny, and L. E. Scriven, *Adv. Mater.* **16**, 1393 (2004).